Nanoscale

PAPER

View Article Online
View Journal | View Issue

Cite this: *Nanoscale*, 2023, **15**, 8377

Luminescent $[CO_2@Ag_{20}(SAdm)_{10}(CF_3COO)_{10}(DMA)_2]$ nanocluster: synthetic strategy and its implication towards white light emission†

Sourav Biswas,‡[a] Anish Kumar Das, ‡[a] Avirup Sardar, [a] Surya Sekhar Manna, [b] Pradip Kumar Mondal,[c] Maurizio Polentarutti,[c] Biswarup Pathak [b] and Sukhendu Mandal *[a]

Owing to the quantized size and associated discrete energy levels, atomically precise silver nanoclusters (Ag NCs) hold great potential for designing functional luminescent materials. However, the thermally activated non-radiative transition of Ag(I)-based NCs has faded the opportunities. To acquire the structurally rigid architecture of cluster nodes for constraining such transitions, a new synthetic approach is unveiled here that utilizes a neutral template as a cluster-directing agent to assemble twenty Ag(I) atoms that ensure the maximum number of surface-protecting ligand attachment possibilities in a particular solvent medium. The solvent polarity triggers the precise structural design to circumvent the over-reliance of the templates, which results in the formation of $[CO_2@Ag_{20}(SAdm)_{10}(CF_3COO)_{10}(DMA)_2]$ NC (where SAdm = 1-adamantanethiolate and DMA = *N*,*N*-dimethylacetamide) exhibiting an unprecedented room-temperature photoluminescence emission. The high quantum yield of the generated blue emission ensures its candidature as an ideal donor for artificial light-harvesting system design, and it is utilized with the two-step sequential energy transfer process, which finally results in the generation of ideal white light. For implementing perfect white light emission, the required chromophores in the green and red emission regions were chosen based on their effective spectral overlap with the donor components. Due to their favorable energy-level distribution, excited state energy transfers occurred from the NC to β-carotene at the initial step, then from the conjugate of the NC and β-carotene to another chromophore, Nile Blue, at the second step *via* a sequential Förster resonance energy transfer pathway.

Received 9th March 2023,
Accepted 7th April 2023

DOI: 10.1039/d3nr01107k

rsc.li/nanoscale

Introduction

Photoluminescence (PL) is one of the most intriguing properties of noble metal nanoclusters (NCs), as their atomic precision in the sub-nanometer region and molecular-like discrete electronic energy levels distinguish them from their plasmonic nanoparticle counterparts.[1–3] PL is susceptible to the size, shape, and structures of the NCs, which can be tuned by modifying the ligands, reaction conditions, solvents, and templating agents.[4–8] Of them, templates mostly control the effective synthesis of Ag(I)-based NCs.[3] In contrast to Ag(0)/Ag(I)-based NCs, Ag(I) clusters are mostly synthesized *via* a self-assembly process in the absence of reducing agents.[9–11] However, the uncontrolled growth of the self-assembly followed by the fast nucleation kinetics of the metal precursors makes the precise structural design challenging, and the introduction of a structure-directing agent appears crucial. However, anionic templating agents have mostly been studied to govern the self-assembly process of Ag(I) cluster node formation through electrostatic attraction and the number of attachments of the surface-protecting ligands.[12–16] Nevertheless, this troublesome control process usually results in non-luminescent Ag(I) NCs at room temperature, where the number of Ag(I) atoms in the cluster node is ≤ 20.[17–21] Their inactivity in PL emission is mostly attributed to the dominance of thermally activated non-radiative transitions, which depend on the surface molecular vibration of the NCs.[20] To overcome the issue, several strategies have been applied to generate PL, such as lowering the temperature to 77 K or imposing structural rigidity through post-synthetic modification.[18,20,22] Unfortunately, room-temperature PL emission was not achieved. It was also observed that changing the bulkiness of the thiolate ligands in an Ag_{16}

[a]*School of Chemistry, Indian Institute of Science Education and Research Thiruvananthapuram, Kerala 695551, India. E-mail: sukhendu@iisertvm.ac.in*
[b]*Department of Chemistry, Indian Institute of Technology Indore, Madhya Pradesh 453552, India*
[c]*Elettra-Sincrotrone Trieste, S.S. 14 Km 163.5 in Area Science Park, Basovizza, Trieste 34149, Italy*

†Electronic supplementary information (ESI) available. CCDC 2210204. For ESI and crystallographic data in CIF or other electronic format see DOI: https://doi.org/10.1039/d3nr01107k

‡The authors made equal contribution.

NC does not guarantee PL emission.[17,18] Thus, the formation of Ag(I) NCs with a constrained structural architecture by incorporating more surface-protecting ligands while retaining the cluster nodes may be more promising to mitigate the dominant non-radiative transitions. However, the incorporation of a larger number of surface-protecting ligands requires charge modification of the anionic templates, whereas varying the nature and structure of the templates leads to the formation of different cluster nodes.[3,10,23] Thus, a synthetic strategy should be designed in such a way that the number of self-assembled Ag(I) atoms is independent of the electronic environment of the template and, finally, can generate PL properties at room temperature.

Ag_{20} NCs have been synthesized several times in the literature by changing their ligands.[19–21,22] However, in all previous cases, the Ag(I) cluster nodes were formed by encapsulating the anionic CO_3^{2-}, irrespective of their ligand architecture, and this fixed the number of ligands attached. Moreover, in our recent work, we obtained neutral CO_2 as a template for the first time in Ag(I) NC synthesis in a controlled synthetic process.[23] However, charge neutralization in that case occurred by connecting the two peripheral motifs at the cluster nodes rather than increasing the number of surface-protecting ligands. Thus, the formation of constrained structural architectures incorporating a greater number of surface-protecting ligands is currently unavailable.

The utilization of the PL emission of the quantized materials is mostly limited to sensing and imaging applications.[1,24–28] Although there has been a recent surge in optoelectronic applications of this unique property, many scopes are still available.[14,29–32] The designing of white light-emitting materials has gained tremendous attention recently for widening the optoelectronic applicability of fluorophores through the Förster resonance energy transfer (FRET) process.[33–37] Generating white light emission through the FRET process primarily requires the conjugation of different fluorescence colors, including red–green–blue (RGB).[38,39] Efficient energy transfers between donors and acceptors containing specific emission colors are also required, which are mostly governed by their inter-component proximity and their interactions. However, the low emission quantum yield and aggregation of their individual components make it more challenging to attain an efficient FRET process in this field.[40–42] Moreover, it is also difficult to control the sequential energy transfer (SET) among the short-wavelength emission (between blue to green) and the long-wavelength emission (between green to red) without relating their structural properties.[43,44] We have already shown that the excellent spectral quality of precisely structured ultra-small Ag(I) NCs makes these suitable as a component for artificial light-harvesting system (LHS) generation.[18] However, there are no reports yet where the emission properties of the Ag (I) NCs are utilized in generating white light emission.

Here, we design a strategy for utilizing a neutral template to assemble Ag(I) atoms with the maximum number of surface-protecting ligand attachment possibilities, resulting in the formation of $[CO_2@Ag_{20}(SAdm)_{10}(CF_3COO)_{10}(DMA)_2]$ (Ag_{20}-SAdm) NC. This approach imposes more rigidity on the metal cluster node through stronger non-covalent interactions that ultimately turn-on the room-temperature blue emission properties. The generated emission of this as-synthesized NC was utilized as a component for a perfect white light emission through a two-step sequential FRET process with the other two selected chromophores, β-carotene and Nile Blue, respectively. Electrostatic interactions and spectral matching between components ensure the achievement of sufficient energy transfer between donor and acceptor at each step for the design of superior artificial LHSs.

Experimental

Synthesis of Ag_{20}-SAdm NC

At room temperature, equimolar amounts (0.1 mmol) of premade $[Ag\text{-}SAdm]_n$ complex[18] and $AgCF_3COO$ were stirred together in the presence of 3 mL (5 : 1) DMA/toluene mixture until a clear solution was obtained. Then, the clear solution was kept in ambient conditions to undergo crystallization. Block-shaped colorless crystals were obtained after six days (yield: 65% Ag-based). Keeping the resultant solution in a desiccator under N_2 atmosphere, no crystals were identified after 14 days. A similar reaction with only DMA as the solvent resulted in no crystals even after 14 days. However, ESI-MS analysis of the resultant mixture confirmed the presence of $[CO_2@Ag_{20}(SAdm)_{10}(CF_3COO)_8(DMA)_4]^{2+}$ NC (Fig. S1†).

Results and discussion

Synthetic strategy

A facile one-pot synthetic reaction between the two Ag(I) precursors was strategically designed here by choosing a specific DMA/toluene solvent mixture (Scheme 1). This is because when only DMA solvent was utilized in the synthesis, the unstable cationic $[CO_2@Ag_{20}(SAdm)_{10}(CF_3COO)_8(DMA)_4]^{2+}$ species was detected by ESI-MS measurements, even though other reaction conditions were the same (Fig. S1†). Colorless block-shaped crystals, obtained from DMA/toluene solution, were structurally elucidated by a single-crystal X-ray diffractometer using a synchrotron source (Fig. S2†). The interpretation of crystal data reveals the overall composition of the crystal, $[CO_2@Ag_{20}(SAdm)_{10}(CF_3COO)_{10}(DMA)_2]$, which crystallizes in a monoclinic crystal system with a space group of $P2_1/n$

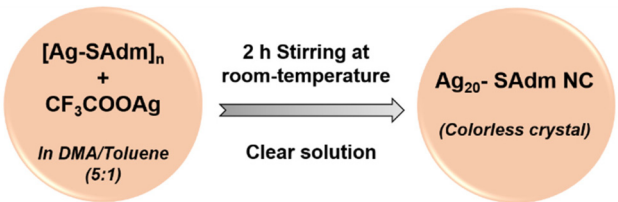

Scheme 1 Schematic representation of Ag_{20}-SAdm NC synthesis.

(No. 14) (Table S1† and Fig. 1). It was found that 20 Ag(I) atoms form a self-assembled doughnut-like core geometry with a CO_2 molecule in the center as a template, where argentophilic interactions help to hold the twenty Ag(I) atoms together. $Ag^I \cdots Ag^I$ bond distances fall in the range of 3.04–3.28 Å.[45] Further, the non-covalent interaction (NCI) calculation through reduced density gradient analysis reveals the existence of the argentophilic interactions (Fig. S3†).[46] As we did not add any precursor of the template, it comes from the aerial source because the reaction was performed in the open air. However, all of the previously reported Ag_{20} NCs contain CO_3^{2-} as a template, but the presence of neutral CO_2 here highlights the uniqueness of our synthetic approach.[19–22] The utilization of DMA in the reaction medium stops the conversion of the aerial CO_2 to CO_3^{2-} inside the reaction mixture, as we observed in our previous work.[23] The absence of the desired product in a controlled experiment inside a desiccator under N_2 atmosphere suggests the significance of the template source for Ag_{20}-SAdm NC synthesis.

Structural illustration

The Ag_{20} cluster node adopts the geometry of the Johnson solid category, delegated as a pentagonal gyrobicupola (J_{31}) which can be demonstrated as a combination of three planes (Fig. 2a and b).[47] Two pentagonal planes are connected to the intermediate decagonal plane by ten square and ten triangular facets, which eventually construct a pentagonal gyrobicupola geometry-like Ag_{20} cluster node (Fig. 2c, d and e). Moreover, a neutral CO_2 molecule is accommodated at the center of the cluster node, resulting in an Ag_{20} core with a CO_2 template (Fig. 2f). Interestingly, the presence of the same number (ten) of the main surface protecting ligands ($^-$SAdm) and auxiliary ligands (CF_3COO^-) makes the as-synthesized Ag_{20}-SAdm NC unique compared to the other reported Ag_{20} NCs (Fig. 2g and h).[19–21] The inclusion of toluene in DMA reduces the polarity of the solvent medium, which facilitates the attachment of additional auxiliary ligands to the cluster node. In the structure, the S atoms of the $^-$SAdm ligands are preferentially located on the square facets of the cluster node in μ_4 bridging mode (Fig. 2g). Out of the ten, eight μ_2 CF_3COO^- ligands are connected to the decagonal plane with Ag–O bond distances of 2.21 Å to 2.46 Å, and two μ_1 CF_3COO^- ligands are attached to the remaining pentagonal planes of the cluster node with Ag–O bond distances of 2.59 Å (Fig. 2h).

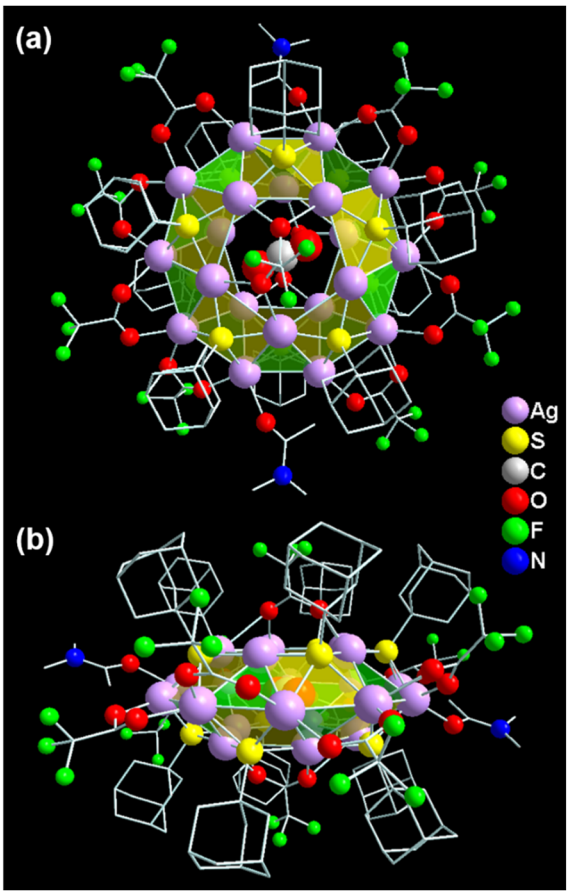

Fig. 1 Obtained crystal structure of the Ag_{20}-SAdm NC: (a) top view and (b) side view.

Spectroscopic and microscopic characterization

Interestingly, in the positive mode ESI-MS spectrum of the as-synthesized crystal, we obtained the highest m/z peak at 5179.76 that can be assigned to the formula $[\{CO_2@Ag_{20}(SAdm)_{10}(CF_3COO)_{10}(DMA)_2\} + H^+]$ (Fig. 3). The isotropic pattern of the obtained peak exactly matched the simulated isotropic pattern of the assigned formula unit. The isotropic distribution of the peaks with $\Delta m/z = 1$ confirms the neutral charge of the formula unit of the synthesized NC. However, the charge state of the species is carried by H^+. Three more prominent peaks are detected with similar isotropic distributions. The experimental isotropic patterns of these three fragments match the simulated patterns well. The peak in the lowest m/z region certainly confirms the presence of CO_2 in the cluster formula unit, as the fragments indicate the release of CO_2 from the cluster node. The XPS survey spectrum indicates the presence of Ag, S, F, O, N, and C in the cluster (Fig. S4 and S5†), which is also corroborated by the EDS analysis (Fig. S6†). Further, the binding energy spectra of each element confirms their corresponding oxidation states (Fig. S5†). The binding energy spectrum of Ag 3d confirms that all the metals here are in the +1 oxidation state. Hence, the overall charge of the cluster node is balanced by the presence of twenty ligands on the surface.

Optical properties

The estimated solid-state bandgap energy was found to be 1.61 eV, measured using the Kubelka–Munk function, which is in good agreement with the theoretical bandgap value of 1.49 eV (Fig. S7 and S8†).[48] The bandgap value is consistent with time, even after one month of synthesis (Fig. S9a†). In addition, the relatively unchanged bandgap value of the NC after exposure to sunlight for fifteen hours demonstrates the extent of its photostability under ambient conditions (Fig. S9b†). Also,

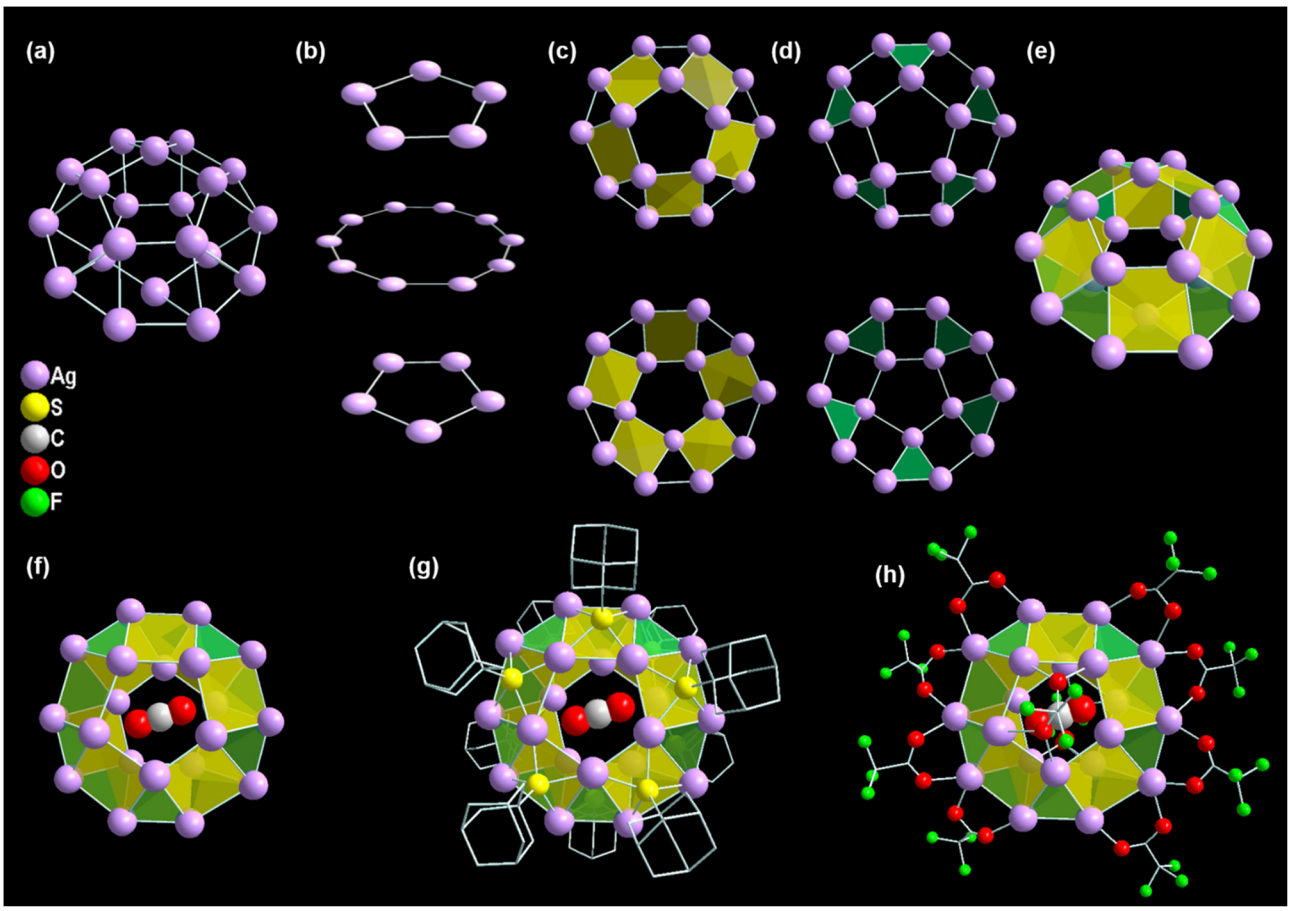

Fig. 2 Structural anatomy of the Ag_{20}-SAdm NC: (a) the arrangement of twenty silver atoms, (b) three planes that construct the geometrical architecture of the cluster node, (c) and (d) ten squares and ten triangular facets which connect the intermediate plane to the other two planes, (e) overall pentagonal gyrobicupola geometry of the cluster node, (f) Ag_{20} cluster node with the CO_2 template, (g) connectivity of $^{-}$SAdm units on the square facets of the pentagonal gyrobicupola geometry with Ag–S bond distances of 2.36–2.61 Å, and (h) attachment of CF_3COO^{-} units on the cluster node.

thermogravimetric analysis (TGA) confirmed that the structural integrity of Ag_{20}-SAdm NC is retained up to 130 °C (Fig. S10†). A featureless absorbance spectrum was observed in the solution phase (DMA medium), which matched the simulated spectrum obtained from the time-dependent density functional theory (TD-DFT) calculation (Fig. 4a). Kohn–Sham molecular orbital analysis revealed that the band at 350 nm originates from HOMO−10 → LUMO and the band at 385 nm originates from HOMO−4 → LUMO (Fig. 4b). The frontier Kohn–Sham orbital population further indicates that the occupied orbitals have a major contribution to the s- and p-like states of the ligand, whereas the unoccupied orbitals are constructed with a major contribution from the s-, p-, and d-like states of the Ag(I) cluster node (Fig. 4c). Hence, the ligand-to-cluster node charge transition is taking place, which is consistent with all other reported Ag_{20} NCs.[19–21] However, most interestingly, in contrast to the reported literature, we observed a strong room-temperature (298 K) PL emission with an emission maximum at 425 nm after exciting the solution at 385 nm (Fig. 4d).[19–21] The relative quantum yield of this emission is ~0.32, and the emission lifetime at the emission maximum (425 nm) is 5.29 ns (inset: Fig. 4d). In addition, Bader's quantum theory of atoms in molecules (QTAIM) calculations confirmed that the accommodation of additional ligands imposes more skeletal rigidity on the cluster nodes.[49] Compared with the reported Ag_{20} NCs, the as-synthesized Ag_{20}-SAdm NC has the highest bond critical points [$\rho(r_c)$ = 0.03216] and Laplacian of the electron density [$\nabla^2\rho(r_c)$ = 0.09844] in Ag···Ag, suggesting very strong non-covalent interactions between two adjacent Ag atoms (Fig. 4e and S11†).[19,20] Hence, we expect that the enhanced bonding character imposes more rigidity on the Ag(I) skeleton, which will help to confine the cluster node vibrations suppressing the non-radiative decay process, ultimately leading to room-temperature PL emission. The effect of the skeletal rigidity is further envisioned by the reduction in the cluster node diameter compared to the previously reported Ag_{20} NCs (Fig. S12†).[20] To quantify the surface molecular vibrations in the DMA medium, we performed a temperature-dependent PL emission study and observed a sharp decrease in PL intensity with the gradual increase in

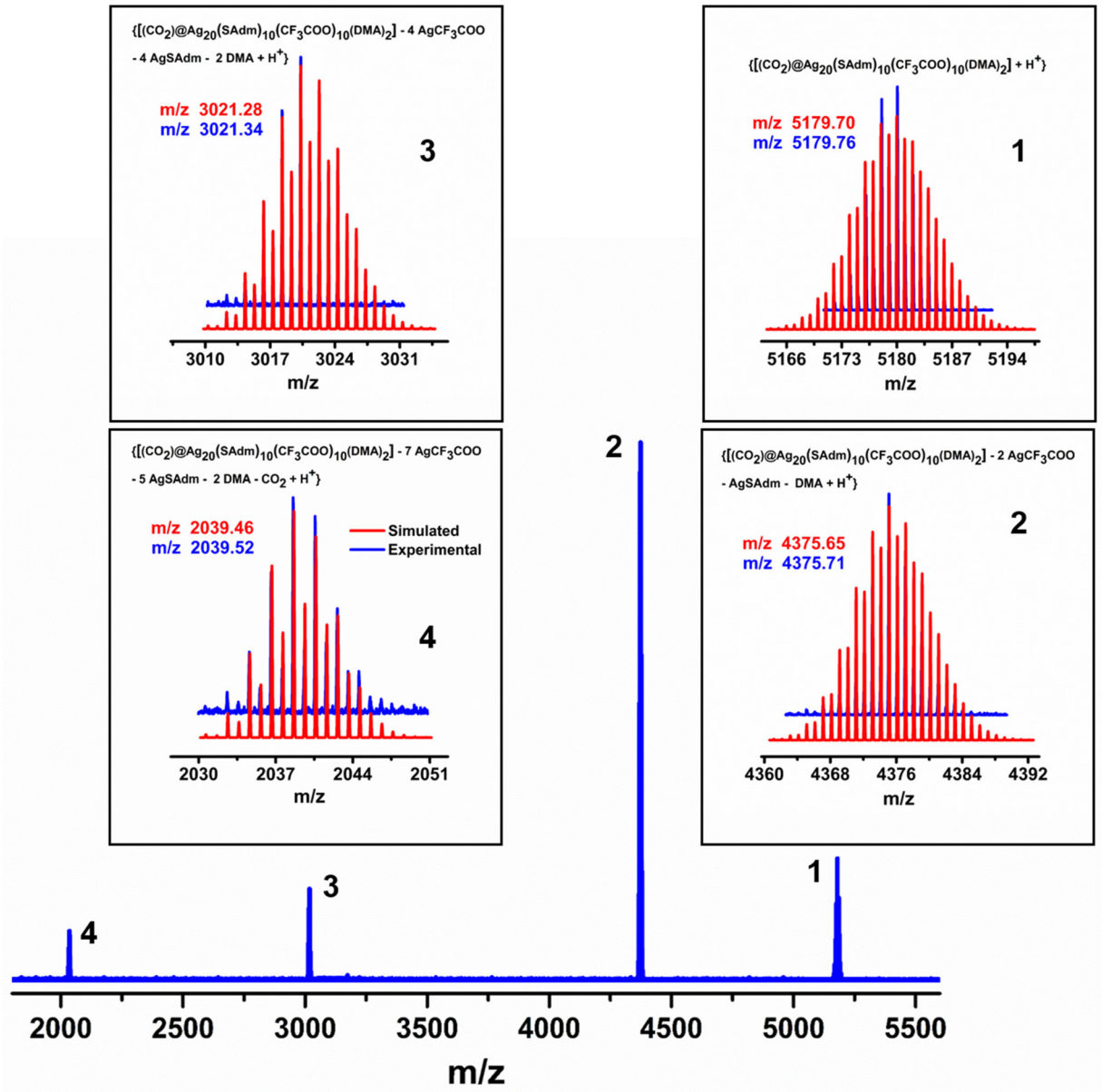

Fig. 3 ESI-MS spectrum of the Ag_{20}-SAdm NC along with its associated fragments. The inset shows a good agreement between the experimental and simulated patterns of each peak.

temperature (up to 343 K) without any emission shift (Fig. 4f). The associated reduction in the PLQY and the emission lifetime indicates the elevation of temperature-driven non-radiative transitions. The estimated radiative and non-radiative rates quantify the cluster node rigidity imposed by the structural architecture (Table S2†). In addition, we conducted temperature-dependent emission studies of the as-synthesized Ag_{20}-SAdm NC in the solid state. Similarly, we observed a gradual decrease in PL intensity with the increase in temperature (Fig. S13†). However, the PL maxima is shifted to 516 nm, which is red-shifted compared to its solution state PL emission maxima. This red shift is clearly attributed to the bandgap values of the NC in the solid state as well as in the solution state. According to the Kohn–Sham diagram, it was determined that the HOMO–LUMO gap of the NC in the solution state is about 3 eV, whereas the PDOS calculation revealed that the optical bandgap of the as-synthesized NC in the solid state is 1.49 eV.

White light emission

After achieving blue PL emission at room temperature, we utilized it for artificial LHS generation.[50–52] The high luminescence quantum yield and the intense blue emission of the discrete Ag_{20}-SAdm NC with proper structural correlation make this a perfect donor for the fabrication of an artificial LHS.[42,53] Here, we have strategically chosen green-emissive β-carotene as

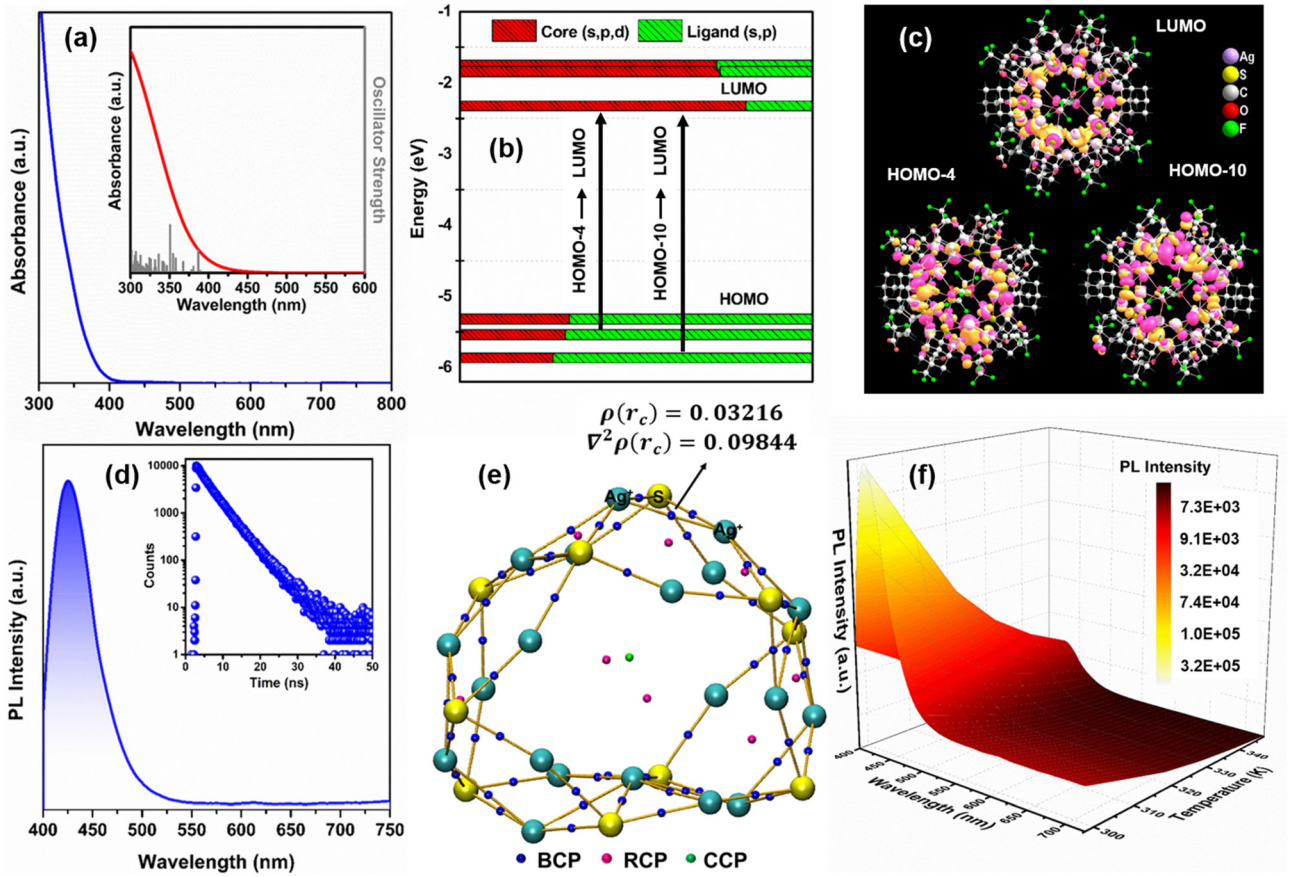

Fig. 4 (a) UV–vis absorbance spectrum of the as-synthesized Ag_{20}-SAdm NC in DMA medium, where the inset shows the simulated absorbance spectrum with oscillator strength; (b) Kohn–Sham diagram and the associated transitions; (c) frontier molecular orbitals (FMOs) of the associated energy states; (d) emission spectrum of the NC in DMA medium upon excitation at 385 nm, where the inset shows the emission lifetime of the NC; (e) QTAIM molecular plot of the bond critical point (BCP), ring critical point (RCP,) and cage critical point (CCP) for considering the Ag···Ag non-covalent interaction (ligands are omitted for clarity); and (f) 3D surface plot of the temperature-driven PL emission of the as-synthesized NC in DMA medium, where the PL intensities vary with the temperature.

a first acceptor due to its spectral overlap with Ag_{20}-SAdm NC (Fig. 5a). From eqn (S1),† we calculated the overlap integral between this donor–acceptor pair to be 6.83×10^{15} M^{-1} cm^{-1} nm^4.[53,54] To comprehend the energy transfer between Ag_{20}-SAdm NC and β-carotene through the FRET mechanism, we examined the emission intensities of the Ag_{20}-SAdm NC (2 mL, 10^{-5} M solution in DMA) after the gradual addition of β-carotene (25 μL of 2×10^{-6} M each time) upon excitation at 385 nm. This causes the emission intensities of Ag_{20}-SAdm NC to continuously drop at 425 nm, while progressively producing a secondary emission with an emission maximum at 540 nm (Fig. S14†). However, the emission of β-carotene was negligible without the antenna of the Ag_{20}-SAdm NC under the same excitation, excluding the possibility of any direct emission of β-carotene (Fig. S15†). The CIE plot obtained from this donor–acceptor pair indicates its insufficiency in generating white light (Fig. S16†). Thus, we decided to construct a SET system by choosing another chromophore, Nile Blue, whose absorption matches with emission of the (Ag_{20}-SAdm NC + β-carotene) conjugate (Fig. 5b). The estimated overlap integral of these two components is 6.66×10^{15} M^{-1} cm^{-1} nm^4 (using eqn (S1)†). During the gradual addition of Nile Blue (10 μL of 2×10^{-6} M each time) to the conjugate, the initial emission intensity remains constant at 425 nm upon excitation at 385 nm. However, another emission is progressively generated at 654 nm, with a gradual dip in the emission intensities at 540 nm (Fig. S17†). Ultimately, a very broad resultant emission spectrum (400–750 nm) is observed under a single excitation wavelength (Fig. 5c), which exhibits intense emission from the three fundamental colors (RGB) essential for white light emission.[39,44] The generation of white light emission is envisioned here by the controlled addition of these chromophores into the Ag_{20}-SAdm NC and appears on the CIE plot with a perfect coordinate (0.33, 0.33) (Fig. 5d). Along with the emission intensities, emission lifetimes are also suppressed sequentially by the addition of these chromophores, which indicates a two-step SET phenomenon. After the addition of 125 μL of 2×10^{-6} M β-carotene in 2 mL of 10^{-5} M Ag_{20}-SAdm NC in DMA, the average emission lifetimes at the 425 nm emission maxima decrease from 5.29 ns to 1.23 ns (Fig. 5e).

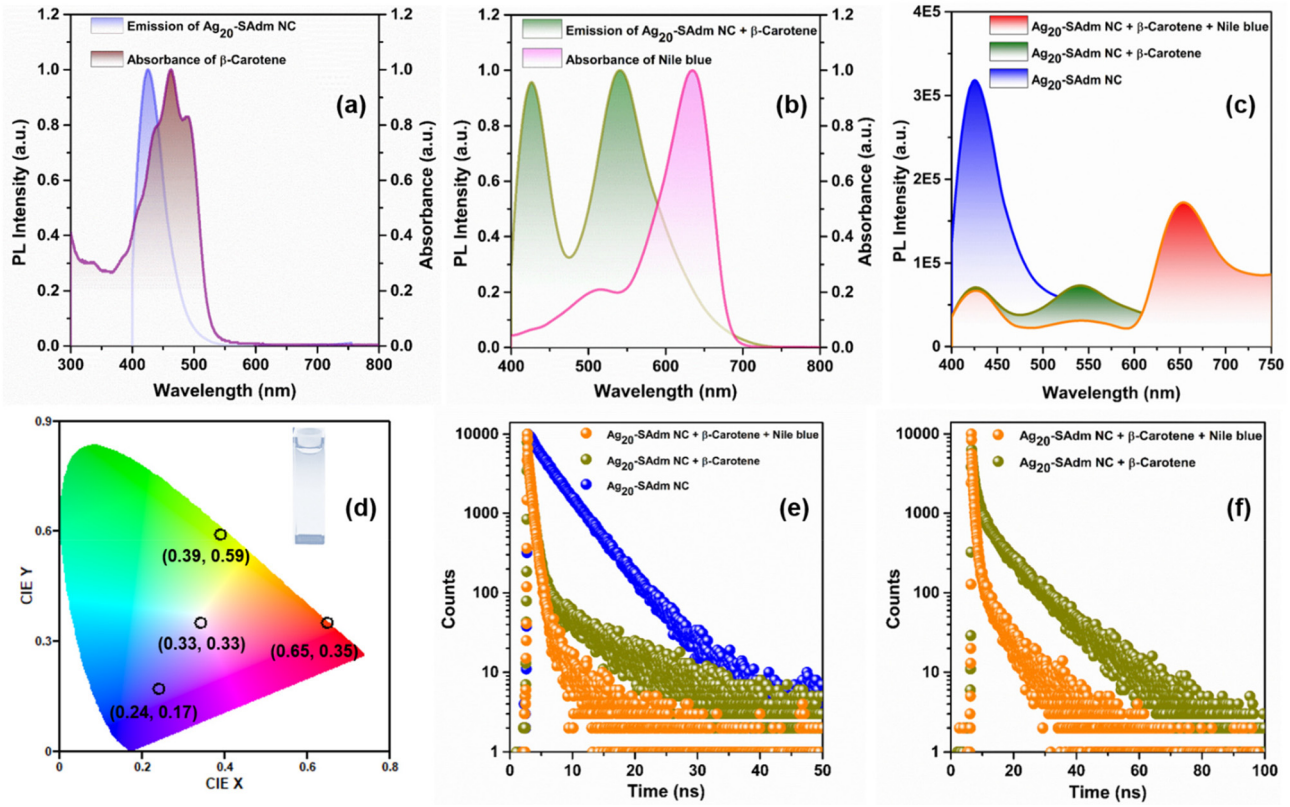

Fig. 5 (a) Spectral overlap between the normalized emission of the Ag_{20}-SAdm NC upon excitation at 385 nm and the normalized absorbance of β-carotene in DMA medium; (b) spectral overlap between the normalized emission of the Ag_{20}-SAdm NC + β-carotene conjugate upon excitation at 385 nm and the normalized absorbance of Nile Blue in DMA medium; (c) emission spectra of corresponding donors and acceptors associated with the generation of white light; (d) change in 1931 CIE chromaticity coordinates after the incorporation of each component in a preferred concentration, where the inset shows the corresponding emission image of the final conjugate under irradiation with a UV–light source; (e) and (f) emission lifetimes of the pure NC and its conjugates at the emission maxima of 425 nm and 540 nm, respectively.

Then, following eqn (S2),† we estimated the energy transfer efficiency of step 1 to be ~77%.[54,55] Further addition of 50 μL of 2×10^{-6} M Nile Blue into the system has little effect on the lifetime of the 425 nm emission maxima; however, it significantly reduces the lifetime of the 540 nm emission maxima from 0.65 ns to 0.27 ns, indicating that the energy transfer efficiency of step 2 is ~59% (Fig. 5f). Thus, it is evident that a two-step SET took place from the Ag_{20}-SAdm NC to β-carotene and then to the Nile Blue in relay mode, designing a perfect LHS for ideal white light emission.

Mechanism of white light emission

Since the individual donor and acceptor components were chosen by matching their emission and absorption bands, we expect the energy transfer to take place through the FRET process. We assume that, initially, β-carotene will attach to the surface of the Ag_{20}-SAdm NC, then the addition of Nile Blue accommodates it on the outer surface due to their difference in surface zeta potential values in the DMA medium (Fig. S18†). Hence, we anticipate that their opposite surface zeta potential values in DMA solvent provide a driving force based on the electrostatic interactions for the conjugation of the Ag_{20}-SAdm NC with dye molecules. Interestingly, the unchanged absorption spectra of the individual components after the sequential addition of these chromophores indicates the stability of the components in the presence of each other at the ground state (Fig. S19†). Furthermore, it is clear that the energy transfers through the FRET originates exclusively at the excited state of the Ag_{20}-SAdm NC through the formation of an active sphere with the acceptor β-carotene that leads to the quenching of the excited donor before they diffuse apart. This process is pronounced in a relay manner when the acceptors are sequentially added to the system, and is further supported by the difference in the electronic energy level (Scheme 2). The FRET efficiencies of the SET process depend on the radius of the effective sphere, which is estimated by calculating the distance (r) between the donor and acceptor in each step per donor–acceptor pair. For the first energy transfer, the calculated (r) between the Ag_{20}-SAdm NC and β-carotene is 4.56 nm, whereas the Förster radius (R_0) of the effective sphere in step 1 is 5.58 nm (eqn (S3) and (S4)†).[55–59] Similarly, for the second energy transfer, the calculated (r) between the conjugate and Nile Blue is 5.40 nm, whereas the (R_0) of the effective sphere in step 2 is 5.74 nm. This enhancement in the distance between

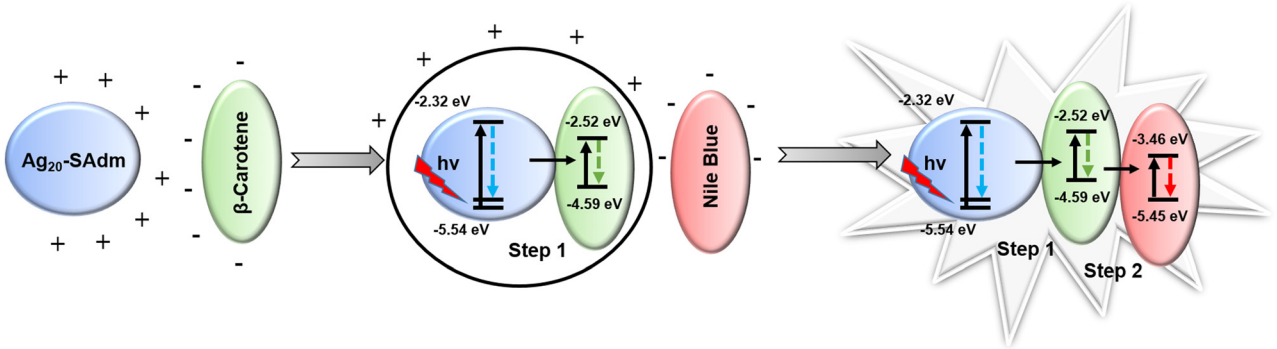

Scheme 2 Proposed mechanism of the two-step FRET process after sequential addition of the chromophores in DMA medium for white light emission.

the two components signifies the sequential addition of the chromophores on the Ag_{20}-SAdm NC, constructing the outer layer of the effective sphere due to electrostatic interactions. The energy transfer rates of the first and second energy transfer processes calculated using eqn (S5)† are 6.33×10^8 s^{-1} and 2.21×10^9 s^{-1}, respectively.[40,44] Hence, the corresponding time scale of these energy transfer rates (1.57 ns and 0.45 ns) is quite predictable from the individual donor lifetime. Therefore, at a favorable position, the acceptor molecule has ample time to efficiently quench the excited state of the donor at every step. Thus, it is clear that upon excitation, the excited Ag_{20}-SAdm NC can transfer energy promptly to the immediately adjacent β-carotene, which is again transferred to the adjacent Nile Blue, thereby quenching the previous excited steps as explained in Scheme 2. Thus, the Ag_{20}-SAdm NC successfully serves as a primary donor for the two-step SET process. Now, this two-step SET process enables the conjugate system to simultaneously exhibit different required emissions at a single excitation, playing a pivotal role in generating the white light emission.

Conclusions

In summary, this study provides a paradigm in template-assisted Ag(I) NC synthesis where the over-reliance of the surface-directing agent on the Ag(I) cluster node and outer surface ligand assembly is becoming obsolete. The controlled reaction condition is facile for the one-pot synthesis of Ag_{20}-SAdm NC, formulated as $[CO_2@Ag_{20}(SAdm)_{10}(CF_3COO)_{10}(DMA)_2]$. In contrast to the reported literature, attachment of a greater number of auxiliary ligands has been purposefully performed here for attaining room-temperature PL emission. The resulting structural rigidity of Ag(I) cluster nodes through stronger non-covalent interactions between adjacent Ag(I) atoms turns on the emission. The resulting intense blue emission is further utilized to design an artificial LHS to generate white light emission through a two-step SET process. The spectral overlap between the donor and acceptors (β-carotene and Nile Blue) at each step makes these selected chromophores compatible with the artificial LHS design. Sequential addition of chromophores to the Ag_{20}-SAdm NC results in a broad emission spectrum containing the three fundamental colors essential for white light emission under a single excitation wavelength. By varying the concentration of chromophores, an ideal white light emission with a CIE coordinate of (0.33, 0.33) is finally produced where the excited state energy transfer efficiencies are 77% in step 1 and 59% in step 2, respectively. Hence, the outcome of this work offers a new strategy to simultaneously control the structural architecture of the Ag(I) cluster for triggering its precise photophysical properties and the utilization of the generated properties. The fundamental investigation of the SET process through an Ag(I) NC-based system will also allow for the discovery of additional opportunities. Thus, we can assume that this work will pave the way for future research into designing functional Ag(I) NCs.

Data availability

The ESI† contains experimental details, crystal data and structure refinement parameters, the ESI-MS spectrum of the unstable cationic NC, the SEM micrograph of the as-synthesized crystal, the reduced density gradient (RDG) isosurface of the argentophilic interaction, XPS and EDS spectra of the Ag_{20}-SAdm NC, bandgap and PDOS calculations of the Ag_{20}-SAdm NC, stability, TGA of Ag_{20}-SAdm NC, the QTAIM molecular plot, the diameter of the Ag_{20} cluster nodes, solid-state PL, the change in emission intensity of the donor molecule, Ag_{20}-SAdm NC with respect to the gradual addition of β-carotene, a comparison of the emission of pure β-carotene with the emission of the Ag_{20}-SAdm NC, the CIE plot obtained from the mixing of Ag_{20}-SAdm NC and β-carotene, the change in emission intensity of the donor molecule, Ag_{20}-SAdm NC + β-carotene conjugate with respect to the gradual addition of Nile Blue, zeta potential values, UV-vis spectrum of Ag_{20}-SAdm NC with the gradual addition of β-carotene followed by the addition of the second chromophore Nile Blue, and references.

Author contributions

Synthesis, characterization, and data interpretation were performed by S. B., A. K. D., and A. S. Computational studies were performed by S. S. M. and B. P. Crystal structure was solved by P. K. M. and M. P. Writing and editing were carried out by S. M. All authors discussed the results and approved the final version of the manuscript.

Conflicts of interest

There are no conflicts to declare.

Acknowledgements

S. B. acknowledges NPDF funding from SERB (PDF/2020/001085).

References

1 X. Kang and M. Zhu, *Chem. Soc. Rev.*, 2019, **48**, 2422–2457.
2 R. Jin, C. Zeng, M. Zhou and Y. Chen, *Chem. Rev.*, 2016, **116**, 10346–10413.
3 I. Chakraborty and T. Pradeep, *Chem. Rev.*, 2017, **117**, 8208–8271.
4 S. Maity, D. Bain and A. Patra, *Nanoscale*, 2019, **11**, 22685–22723.
5 X. Kang and M. Zhu, *Chem. Mater.*, 2019, **31**, 9939–9969.
6 T. Kawawaki, A. Ebina, Y. Hosokawa, S. Ozaki, D. Suzuki, S. Hossain and Y. Negishi, *Small*, 2021, **17**, 2005328.
7 H. Hirai, S. Ito, S. Takano, K. Koyasu and T. Tsukuda, *Chem. Sci.*, 2020, **11**, 12233–12248.
8 Q. Yao, Z. Wu, Z. Liu, Y. Lin, X. Yuan and J. Xie, *Chem. Sci.*, 2021, **12**, 99–127.
9 A. Ebina, S. Hossain, H. Horihata, S. Ozaki, S. Kato, T. Kawawaki and Y. Negishi, *Nanomaterials*, 2020, **10**, 1105.
10 Y. Jin, C. Zhang, X.-Y. Dong, S.-Q. Zang and T. C. W. Mak, *Chem. Soc. Rev.*, 2021, **50**, 2297–2319.
11 W. A. Dar, A. Jana, K. S. Sugi, G. Paramasivam, M. Bodiuzzaman, E. Khatun, A. Som, A. Mahendranath, A. Chakraborty and T. Pradeep, *Chem. Mater.*, 2022, **34**, 4703–4711.
12 Q.-M. Wang, Y.-M. Lin and K.-G. Liu, *Acc. Chem. Res.*, 2015, **48**, 1570–1579.
13 R. Vilar, *Angew. Chem., Int. Ed.*, 2003, **42**, 1460–1477.
14 S. Biswas, A. K. Das, A. C. Reber, S. Biswas, S. Bhandary, V. B. Kamble, S. N. Khanna and S. Mandal, *Nano Lett.*, 2022, **22**, 3721–3727.
15 Y.-M. Su, Z. Wang, C.-H. Tung, D. Sun and S. Schein, *J. Am. Chem. Soc.*, 2021, **143**, 13235–13244.
16 Y.-M. Su, Z. Wang, S. Schein, C.-H. Tung and D. Sun, *Nat. Commun.*, 2020, **11**, 1–9.
17 M. J. Alhilaly, R.-W. Huang, R. Naphade, B. Alamer, M. N. Hedhili, A.-H. Emwas, P. Maity, J. Yin, A. Shkurenko, O. F. Mohammed, M. Eddaoudi and O. M. Bakr, *J. Am. Chem. Soc.*, 2019, **141**, 9585–9592.
18 A. K. Das, S. Biswas, S. S. Manna, B. Pathak and S. Mandal, *Chem. Sci.*, 2022, **13**, 8355–8364.
19 D. Sun, H. Wang, H.-F. Lu, S.-Y. Feng, Z.-W. Zhang, G.-X. Sun and D.-F. Sun, *Dalton Trans.*, 2013, **42**, 6281–6284.
20 S. Yuan, Y.-K. Deng, X.-P. Wang and D. Sun, *New J. Chem.*, 2013, **37**, 2973–2977.
21 K. Zhou, C. Qin, X.-L. Wang, K.-Z. Shao, L.-K. Yan and Z.-M. Su, *CrystEngComm*, 2014, **16**, 7860–7864.
22 S. Li, X.-S. Du, B. Li, J.-Y. Wang, G.-P. Li, G.-G. Gao and S.-Q. Zang, *J. Am. Chem. Soc.*, 2018, **140**, 594–597.
23 S. Biswas, A. K. Das, S. S. Manna, B. Pathak and S. Mandal, *Chem. Sci.*, 2022, **13**, 11394–11404.
24 Y. Xiao, Z. Wu, Q. Yao and J. Xie, *Aggregate*, 2021, **2**, 114–132.
25 Y. Su, T. Xue, Y. Liu, J. Qi, R. Jin and Z. Lin, *Nano Res.*, 2019, **12**, 1251–1265.
26 S. Qian, Z. Wang, Z. Zuo, X. Wang, Q. Wang and X. Yuan, *Coord. Chem. Rev.*, 2022, **451**, 214268.
27 J. Yang and R. Jin, *J. Phys. Chem. C*, 2020, **125**, 2619–2625.
28 A. K. Das, S. Biswas, A. Thomas, S. Paul, A. S. Nair, B. Pathak, M. S. Singh and S. Mandal, *Mater. Chem. Front.*, 2021, **5**, 8380–8386.
29 A. K. Das, S. Biswas, V. S. Wani, A. S. Nair, B. Pathak and S. Mandal, *Chem. Sci.*, 2022, **13**, 7616–7625.
30 M. A. Abbas, R. Thota, K. Pyo, D. Lee and J. H. Bang, *ACS Energy Lett.*, 2020, **5**, 1404–1406.
31 B.-L. Han, Z. Wang, R. K. Gupta, L. Feng, S. Wang, M. Kurmoo, Z.-Y. Gao, S. Schein, C.-H. Tung and D. Sun, *ACS Nano*, 2021, **15**, 8733–8741.
32 Z. Wang, H.-F. Su, Y.-W. Gong, Q.-P. Qu, Y.-F. Bi, C.-H. Tung, D. Sun and L.-S. Zheng, *Nat. Commun.*, 2020, **11**, 1–8.
33 M. A. Abbas, P. V. Kamat and J. H. Bang, *ACS Energy Lett.*, 2018, **3**, 840–854.
34 G. V. Hartland, L. V. Besteiro, P. Johns and A. O. Govorov, *ACS Energy Lett.*, 2017, **2**, 1641–1653.
35 M. Zhang, S. Yin, J. Zhang, Z. Zhou, M. L. Saha, C. Lu and P. J. Stang, *Proc. Natl. Acad. Sci. U. S. A.*, 2017, **114**, 3044–3049.
36 H. Wu, Y. Chen, X. Dai, P. Li, J. F. Stoddart and Y. Liu, *J. Am. Chem. Soc.*, 2019, **141**, 6583–6591.
37 R. N. Dsouza, U. Pischel and W. M. Nau, *Chem. Rev.*, 2011, **111**, 7941–7980.
38 S. Reineke, F. Lindner, G. Schwartz, N. Seidler, K. Walzer, B. Lüssem and K. Leo, *Nature*, 2009, **459**, 234–238.
39 H. Wu, G. Zhou, J. Zou, C. L. Ho, W. Y. Wong, W. Yang, J. Peng and Y. Cao, *Adv. Mater.*, 2009, **21**, 4181–4184.
40 K. Mondal, A. Pramanik, T. Mondal, S. S. Panja, R. Sarkar and P. Kumbhakar, *J. Phys. Chem. Lett.*, 2022, **13**, 3079–3088.
41 Y. Li, S. S. Rajasree, G. Y. Lee, J. Yu, J.-H. Tang, R. Ni, G. Li, K. N. Houk, P. Deria and P. J. Stang, *J. Am. Chem. Soc.*, 2021, **143**, 2908–2919.

42 A. Kumar, R. Saha and P. S. Mukherjee, *Chem. Sci.*, 2021, **12**, 5319–5329.
43 D. Zhang, W. Yu, S. Li, Y. Xia, X. Li, Y. Li and T. Yi, *J. Am. Chem. Soc.*, 2021, **143**, 1313–1317.
44 M. Hao, G. Sun, M. Zuo, Z. Xu, Y. Chen, X. Y. Hu and L. Wang, *Angew. Chem., Int. Ed.*, 2020, **59**, 10095–10100.
45 H. Schmidbaur and A. Schier, *Angew. Chem., Int. Ed.*, 2015, **54**, 746–784.
46 T. Lu and F. Chen, *J. Comput. Chem.*, 2012, **33**, 580–592.
47 N. W. Johnson, *Can. J. Math.*, 1966, **18**, 169–200.
48 G. Kortüm, W. Braun and G. Herzog, *Angew. Chem., Int. Ed. Engl.*, 1963, **2**, 333–341.
49 T. Lu and F.-W. Chen, *Acta Chim. Sin.*, 2011, **69**, 2393–2406.
50 G. McDermott, S. Prince, A. Freer, A. Hawthornthwaite-Lawless, M. Papiz, R. Cogdell and N. Isaacs, *Nature*, 1995, **374**, 517–521.
51 G. D. Scholes, G. R. Fleming, A. Olaya-Castro and R. Van Grondelle, *Nat. Chem.*, 2011, **3**, 763–774.
52 S. Kundu and A. Patra, *Chem. Rev.*, 2017, **117**, 712–757.
53 J. R. Lakowicz, *Principles of fluorescence spectroscopy*, Springer, 2006.
54 M. K. Barman, S. Bhattacharyya and A. Patra, *Phys. Chem. Chem. Phys.*, 2013, **15**, 16834–16840.
55 T. Sen, S. Sadhu and A. Patra, *Appl. Phys. Lett.*, 2007, **91**, 043104.
56 T. Förster, *Ann. Phys.*, 1948, **437**, 55–75.
57 R. C. Powell and Z. G. Soos, *J. Lumin.*, 1975, **11**, 1–45.
58 S. Halivni, A. Sitt, I. Hadar and U. Banin, *ACS Nano*, 2012, **6**, 2758–2765.
59 A. J. Mork, M. C. Weidman, F. Prins and W. A. Tisdale, *J. Phys. Chem. C*, 2014, **118**, 13920–13928.